Available online at www.sciencedirect.com
SCIENCE DIRECT®
Biomaterials 26 (2005) 5632–5639
Biomaterials
www.elsevier.com/locate/biomaterials

Concentrated hydroxyapatite inks for direct-write assembly of 3-D periodic scaffolds

Sarah Michna[a], Willie Wu[a], Jennifer A. Lewis[a,b,*]

[a]*Materials Science and Engineering Department, University of Illinois, Urbana, IL 61801, USA*
[b]*Chemical and Biomolecular Engineering Department, University of Illinois, Urbana, IL 61801, USA*

Received 2 November 2004; accepted 23 February 2005
Available online 21 April 2005

Abstract

Hydroxyapatite (HA) scaffolds with a 3-D periodic architecture and multiscale porosity have been fabricated by direct-write assembly. Concentrated HA inks with tailored viscoelastic properties were developed to enable the construction of complex 3-D architectures comprised of self-supporting cylindrical rods in a layer-by-layer patterning sequence. By controlling their lattice constant and sintering conditions, 3-D periodic HA scaffolds were produced with a bimodal pore size distribution. Mercury intrusion porosimetry (MIP) was used to determine the characteristic pore size and volume associated with the interconnected pore channels between HA rods and the finer pores within the partially sintered HA rods.

Keywords: Hydroxyapatite; Bone tissue engineering; Scaffolds; Direct-write assembly

1. Introduction

There is considerable demand in oral surgery [1–3] and orthopedic medicine [4,5] for inorganic scaffolds suitable for repair or replacement of human bone tissue. Hydroxyapatite (HA), a calcium phosphate-based ceramic material, is an excellent candidate material for such applications [6–9]. Its bioactivity promotes both tissue bonding and new tissue formation. HA implants can be constructed from a variety of methods including hydrothermal conversion from coral [10], use of polymer sponges as molds [11], and bulk ceramic processing techniques [8,12–14]. In the latter case, porosity is introduced by adding organic porogens [8], foaming [12–14], or limiting densification during the sintering process [15]. All of these approaches, however, suffer from a lack of control over the final architecture and distribution of porosity within the HA implant.

Several fabrication approaches have been recently introduced that allow the construction of 3-D HA scaffolds with engineered architecture and porosity [16–20]. Most of these approaches rely on computer-aided design to build structures in a predefined pattern with controlled feature size and geometry without the need for subsequent machining. For example, three-dimensional printing (3DP), which involves ink-jet printing of binder droplets onto a ceramic (or polymeric) powder bed, has been used to create bone scaffolds with minimum feature sizes on the order of several hundred micrometers [17,21]. During 3DP, the spreading and wetting of impinging droplets within the porous powder bed leads to scaffolds with rough surfaces and limited feature resolution. Stereolithography (SLS) has also been used to create HA scaffolds via a lost mold technique [19,20]. In this approach, a laser is rastered across a photocurable monomeric resin to create a negative replica of the desired scaffold structure within a polymeric mold. The scaffold is produced by

*Corresponding author. Materials Science and Engineering Department, University of Illinois, Urbana, IL 61801, USA. Tel.: +1 217 244 4973.
E-mail address: jalewis@uiuc.edu (J.A. Lewis).

0142-9612/$ - see front matter © 2005 Elsevier Ltd. All rights reserved.
doi:10.1016/j.biomaterials.2005.02.040

infiltrating the mold with an HA suspension, drying the structure, removing the organic mold by heating to elevated temperatures, followed by sintering. The organic removal process can be quite lengthy, however, often requiring days to generate scaffolds that are free of defects [22]. Recently, SLS has been used to directly pattern HA scaffolds by laser curing a monomeric resin filled with ceramic particles [16]. Unfortunately, the curing efficiency and feature resolution are considerably lower than that observed for pure resins, because the HA filler particles scatter light.

Direct-write assembly [23–25] using concentrated colloidal inks offers a new approach for creating 3-D periodic HA scaffolds. By carefully tailoring ink composition and viscoelasticity, HA scaffolds can be built with minimal organic content (~1% by weight) without the need for a sacrificial support material or mold. Here, we report the development of concentrated HA inks suitable for direct-write assembly of HA scaffolds comprised of self-supporting, cylindrical filaments (or rods) patterned with varying lattice constant. By tailoring their printed architecture and sintering conditions, HA scaffolds were created with a bimodal pore size distribution, consisting of an interpenetrating 3-D network of large pores between HA rods (characteristic diameter of ~200–500 μm) and finer micropores (<1 μm) within the HA rods. These 3-D periodic HA scaffolds may find potential application as implant materials for bone tissue engineering.

2. Experimental procedure

2.1. Materials system

A commercially available HA powder, $Ca_{10}(PO_4)_6(OH)_2$ (Lot # 13310, Riedel-de Haën, Germany), with an average particle diameter of 2.78 μm, as measured by centrifugal photo-sedimentation (Capa-700, Horiba Instruments Inc., Irvine, CA) and a specific surface area of 75.7 m^2/g, as measured by nitrogen adsorption (ASAP 2400 BET, Micrometrics, Norcross, GA) served as the colloidal phase in our inks. The HA powder was dispersed in deionized water with Darvan 821A (R.T. Vanderbilt Co., Norwalk, CT), a 40 wt% ammonium polyacrylate (PAA) solution. PAA is an anionic polyelectrolyte with a linear backbone comprised of one ionizable carboxylic acid group per monomer unit. Hydroxypropyl methylcellulose (Methocel F4M, Dow Chemical Company, Midland, MI) was added in an amount of 5 mg/mL of solution phase as a viscosifing agent and 1-octanol (Fisher Scientific,Pittsburg, PA) was added as 1 vol% to prevent foaming. Poly(ethylenimine) (PEI) is a highly branched, cationic polyelectrolyte with a 1:2:1 ratio of primary, secondary, and tertiary amines (NH_x). PEI (M_W~600) was supplied (Polysciences, Inc.) as a concentrated liquid (99%), which was diluted with deionized water to form a concentrated aqueous solution (40% by weight) for ink formulation.

2.2. Calcining and milling of hydroxyapatite powders

The influence of calcining and milling conditions on the as-received HA powder was evaluated through specific surface area and particle size analysis, as well as direct imaging by SEM (Hitachi S-4700, Hitachi High Technologies America, Inc., Pleasanton, CA). The HA powder was placed in covered alumina crucibles and ramped to the desired calcination temperature ($T_{calcine} = 400-1100\,^{\circ}C$) at a rate of 20 °C/min and held at temperature for varying times ($t_{calcine} = 0.5$–10 h). The specific surface area of these calcined HA powders was measured using nitrogen gas adsorption (ASAP 2400 BET, Micrometrics, Norcross, GA). From the data, an optimal calcination temperature of 1100 °C was determined. The as-received and calcined powders were also examined by X-ray diffraction (Rigaku D-Max, Rigaku Corporation, Japan) to ensure that the calcination process did not alter the HA crystal structure.

Calcined HA powder was ball-milled to break up particle agglomerates, which yielded a two-fold decrease in mean particle size. A 500 mL high-density polyethylene bottle (Nalgene Labware, Rochester, NY) was filled with 250 mL of zirconia grinding media, $\frac{1}{2} \times \frac{1}{2}$. Deionized water with 20 vol% HA powder was added to fill the interstitial volume of the milling media. The mill was placed on a long-roll jar mill (US Stoneware, East Palastine, OH) at 30 rpm for 12 h.

2.3. Hydroxyapatite inks

HA inks were prepared by first making a stable colloidal suspension (30 vol% HA) in deionized water. An appropriate amount of the PAA dispersant (0.57 mg PAA/m^2 HA) was added to deionized water and the pH was adjusted to 9 by the addition of 5 M NH_4OH. At this pH, the PAA species are fully ionized allowing them to impart the desired suspension stability [26]. The ceramic powder was then added to this aqueous solution in three aliquots. The HA suspension was ultra-sonicated for 3 min after adding the first and second aliquots using an ultra-sonicating horn (550 Sonic Dismembrator, Fisher Scientific, Pittsburg, PA) pulsed with 1 s on/off intervals. After adding the remainder of the HA powder, the suspension was placed on a paint shaker (Red Devil 5400, Red Devil Equipment Co., Plymouth, MN) for 30 min followed by ultrasonication for 3.5 min with 1 s on/off intervals.

The stable HA suspension was filtered through a 20 μm nylon mesh (Small Parts Inc., Miami Lakes, FL) to remove any impurities or hard agglomerates, and

then centrifuged (Avanti J-25I, Beckman Instruments, Inc., Fullerton, CA) at 2000 rpm for 60 min to concentrate it to 46–48 vol% HA. The supernatant was decanted and the remaining concentrated HA suspension was placed on the paint shaker for 50 min. The viscosifier and defoamer were then added in the appropriate amounts, followed by shaking for 30 min on the paint shaker. The pH was adjusted again to 9 by the addition of 1 M HNO_3, with an additional 20 min on the paint shaker after each addition. Finally, the suspension was gelled by adding PEI. A few zirconia grinding media, $\frac{1}{4} \times \frac{1}{4}$, were included to improve mixing of the increasingly viscous ink. The HA ink was then placed on the paint shaker for 10 min between each addition of the PEI gelling agent and 30 min after the final addition.

2.4. Rheological measurements

The rheological properties of HA suspensions were measured using a Bohlin CVOR controlled stress rheometer (Bohlin Instruments Limited, Gloucester, England) fitted with a C25 cup and bob geometry (bob diameter of 25 mm and gap width of 0.15 mm), which has a stress range of 2.5×10^{-2}–50 Pa with a lower shear rate limit of $0.05262\,s^{-1}$. The apparent viscosity was measured for HA suspensions of varying volume fractions produced from both as-received and calcined (1100 °C for 10 h)/ball-milled (12 h) powders. In stress viscometry mode, the shear rate data were acquired as a function of shear stress in an ascending series of discrete steps with a 1 min equilibration time at each step. The elastic shear modulus (G') of concentrated HA inks as a function of varying PEI gelling agent addition was measured in oscillatory mode using a Bohlin CS50 controlled stress rheometer (Bohlin Instruments Limited, Gloucester, England) fitted with a C14 cup and vane tool (vane diameter of 14 mm and gap width of 0.15 mm), which has a stress range of 1–750 Pa, with a strain sensitivity of $\sim 10^{-4}$. The stress sweep was performed after allowing each sample a quiescent equilibration time of 1 h. All measurements were carried out at 25 °C using a specially designed solvent trap filled with deionized water to minimize evaporation.

2.5. Hydroxyapatite scaffold fabrication

3-D periodic HA scaffolds were constructed via direct-write assembly of a concentrated HA ink using a robotic deposition apparatus (JL2000 Robocaster, Sandia National Laboratories, Albuquerque, NM). This technique employs an ink delivery system mounted on a z-axis motion-controlled stage for agile printing onto a moving $x-y$ stage. Note, 3-axis motion is independently controlled by a custom-designed, computer-aided direct-write program (Robocad 3.0, 3-D Inks, Stillwater, OK). The ink is housed in a syringe (barrel diameter = 9 mm, EFD, Inc., East Providence, RI) and deposited through a cylindrical deposition nozzle (diameter, D) at the volumetric flow rate ($= 0.25\pi D^2 v$) required to maintain a constant $x-y$ table speed (v). The deposition process was carried out under a non-wetting oil to prevent non-uniform drying during assembly.

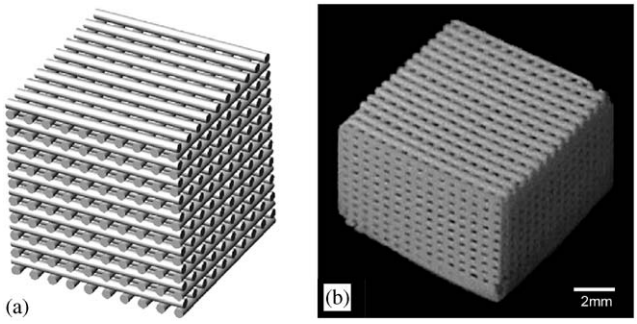

Fig. 1. (a) Schematic illustrations of the 3-D periodic scaffold design and (b) corresponding optical image of a hydroxyapatite scaffold ($6.5 \times 6.5 \times 6\,mm^3$) created by direct-write assembly with center-to-center rod distance of 500 μm.

Three-dimensional periodic HA scaffolds ($6 \times 6 \times 6\,mm^3$) were assembled ($D = 250\,\mu m$, $v = 3\,mm/s$, $\Delta z = 0.98D$), which consisted of a linear array of parallel rods aligned with the x- or y-axis such that their orientation was orthogonal to the previous layer (see Fig. 1). The center-to-center rod spacing (L) was varied from 250 to 750 μm, which corresponds to a minimum separation distance (D_{rod}) between rods ranging from 0 to 500 μm. Once a given layer is constructed, the nozzle is translated up a distance Δz and another layer is deposited. This process is repeated until the entire scaffold has been printed. After assembly is completed, the oil is drained from the part and the scaffold is allowed to dry uniformly in air. Note, solid HA scaffolds ($D_{rod} = 0\,\mu m$) were also constructed, which served as a benchmark for evaluating the effects of sintering temperature on HA densification.

2.6. Sintering and characterization of hydroxyapatite scaffolds

HA scaffolds were sintered at various temperatures (1200–1300 °C) to achieve the desired degree of densification. This temperature range was utilized, because it promotes HA densification without decomposition [15,27]. Specifically, the HA scaffolds were heated at 1 °C/min to 400 °C for 1 h, then at 3 °C/min to 900 °C for 2 h, and, finally, at 10 °C/min to the sintering temperature (hold time = 2 h). The sintered HA scaffolds were characterized by X-ray diffraction (Rigaku D-Max, Rigaku Corporation, Japan) to determine whether any phase changes occurred during this process. The

scaffolds were also imaged using scanning electron microscopy (SEM) (Ziess DSM 960, Carl Zeiss, Inc., Germany) to evaluate their microstructural evolution. The pore size distribution and final pore volume of representative 3-D periodic HA scaffolds ($D_{rod} = 250\,\mu m$) were characterized by mercury intrusion porosimetry (MIP) (AutoPore II 9220, Micromeritics, Norcross, GA). In addition, the sintered density (ρ_s) of 3-D solid HA scaffolds ($D_{rod} = 0\,\mu m$) was characterized using the Archimedes' method [28]. Their sintered density and open porosity were determined by:

$$\rho_s = \frac{M_{dry}}{(M_{sat} - M_{susp})}\rho_{water}, \quad (1)$$

$$\text{Open Porosity } (\%) = \frac{(M_{sat} - M_{dry})}{(M_{sat} - M_{susp})}100\%, \quad (2)$$

where M_{dry} is the scaffold mass, M_{sat} the scaffold mass measured in air after immersion in boiling deionized water for 2 h prior to cooling to room temperature, and M_{susp} the mass found by suspending the saturated scaffold in deionized water.

3. Results and discussion

3.1. Calcining and milling effects on hydroxyapatite powder properties

The as-received HA powder had a specific surface area (SSA) of 75.7 m^2/g. Upon calcining at 1100 °C for 10 h, there was a dramatic change in powder morphology yielding a final SSA value of 3.8 m^2/g. Even though the most significant SSA reduction occurred upon calcining at 1100 °C for ~0.5 h (see Fig. 2(a)), the optimal powder morphology emerged only after calcining at this temperature for several hours. This can be seen in the accompanying SEM images shown in Fig. 2(b), which reveal the morphological evolution observed for representative HA particles as a function of calcination time at 1100 °C. Longer times (~10 h) are clearly required for these particles to adopt the nominally smooth, pore-free morphology, which is considered optimal for creating concentrated HA inks for direct-write assembly.

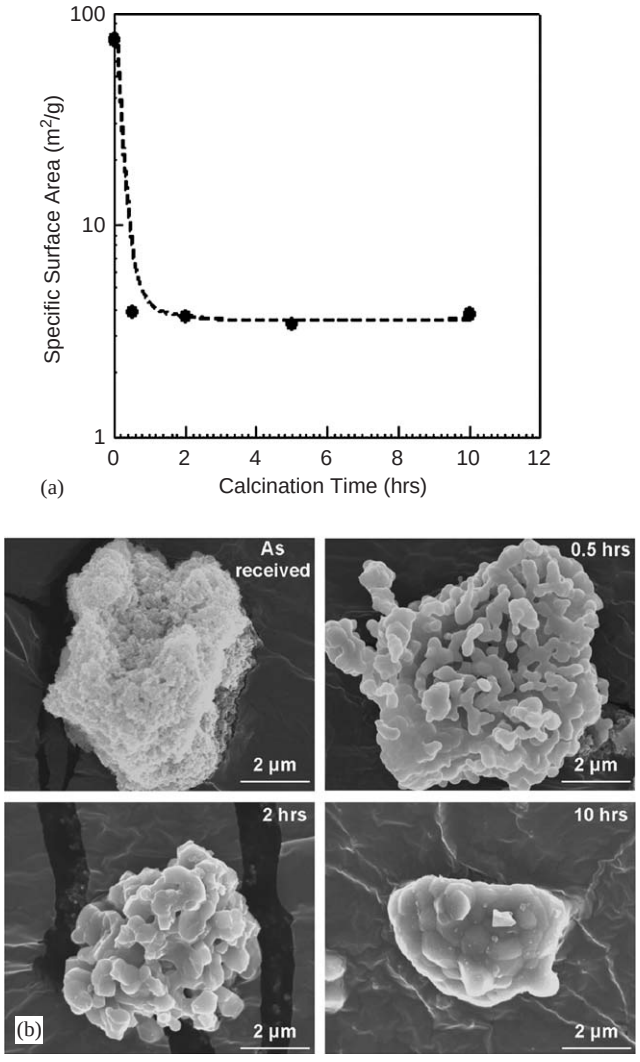

Fig. 2. (a) Plot of specific surface area of hydroxyapatite powder as a function of calcination time at a fixed temperature of 1100 °C, and (b) SEM micrographs of individual particles from the as-received and calcined (at 1100 °C) hydroxyapatite powder at varying hold times.

3.2. Rheological properties of concentrated hydroxyapatite suspensions

The relative suspension viscosity (η_{rel}) is a sensitive probe of the effects of particle stability and morphology on flow behavior. For model systems comprised of dense, monodisperse hard spheres, η_{rel} is given by the Krieger–Dougherty (K–D) relationship [29]:

$$\eta_{rel} = \frac{\eta_{app}}{\eta_0} = \left(1 - \frac{\phi}{\phi_{max}}\right)^{-K\phi_{max}}, \quad (3)$$

where η_{app} is the apparent suspension viscosity, η_0 the solution viscosity, ϕ the colloid volume fraction, ϕ_{max} the maximum colloid volume fraction (~0.6–0.64 corresponding to random close packing of hard spheres), and K the hydrodynamic shape factor (= 2.5 for monodisperse hard spheres). One can therefore use Eq. (3) to determine the ideal value of η_{rel} as a function of ϕ depicted by the solid curve shown in Fig. 3. For comparison, we also report the measured values of η_{rel} as a function of ϕ_{HA} for suspensions produced from both as-received and optimized (calcined and milled) HA powders (see Fig. 3). Note, the short dashed lines are fits to these data using a modified form of the K–D relationship, where ϕ_{max} and K are now fitting parameters. The effects of HA particle morphology are evident from both the magnitude of η_{rel} as well as the value of these parameters (i.e., ϕ_{max}~0.35, $K = 11$ for

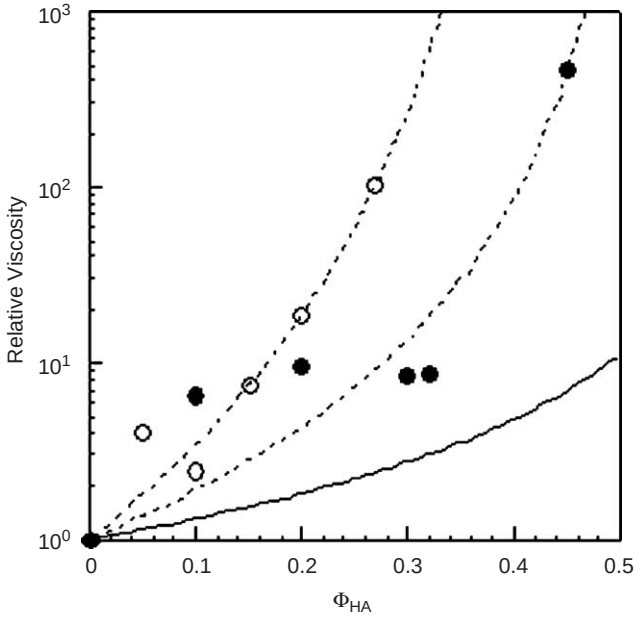

Fig. 3. Semi-log plot of the relative viscosity (η_{rel}) of hydroxyapatite suspensions as a function of hydroxyapatite volume fraction prepared from as-received (○) and calcined (●) hydroxyapatite powder. [Note: Dashed lines represent K–D fits to these data, where $\eta_o = 0.03$ Pas, $K_{as-received} = 11$, and $K_{calcined} = 6$. Solid line represents the K–D equation where $K = 2.5$.]

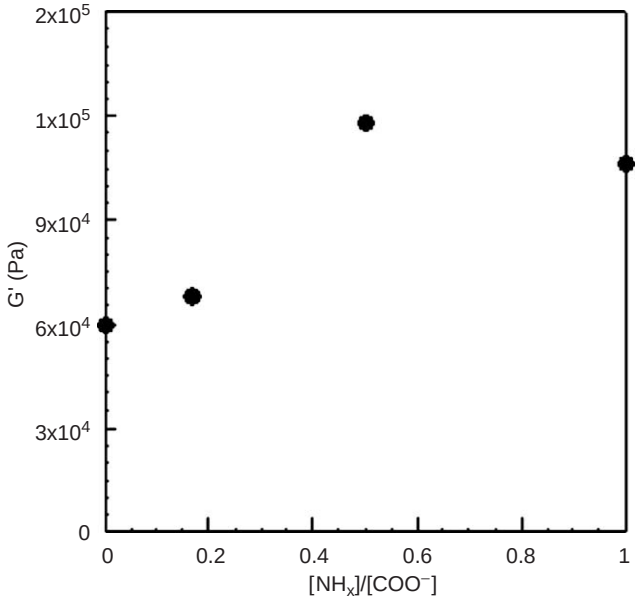

Fig. 4. The elastic modulus (G') as a function of PEI addition, expressed as a ratio of [NH_x]:[COO^-], for concentrated hydroxyapatite suspensions ($\phi_{HA} = 0.45$).

the as-received HA powder and $\phi_{max} \sim 0.5$, $K = 6$ for the calcined HA powder) required to best fit the observed data. Although deviations in K were expected given the non-spherical nature of individual HA particles, the sharp reduction in ϕ_{max} observed for the as-received HA powder is clearly a manifestation of its highly porous nature. Effectively, each individual HA particle acts a "sponge" absorbing liquid, and, thereby, increasing the effective solids loading in suspension. The primary consequence is a sharp decrease in ϕ_{max} from the maximum value of 0.6–0.64 for observed monodisperse hard spheres [29]. By optimizing the HA powder characteristics through calcination and milling, we obtained the high solids loading (~45–50 vol%) required for creating inks for direct-writing of 3-D periodic scaffolds [24].

HA inks were produced by first creating stable HA suspensions ($\phi = 0.45$) followed by flocculation through the addition of a gelling agent, PEI [30], to enhance ink elasticity, as shown in Fig. 4. In this approach, positively charged, amine [NH_x] groups along the PEI backbone interact with negatively charged, carboxylic acid [COO^-] groups along the PAA backbone to induce the desired gelation of PAA-coated HA particles in suspension [30]. Interestingly, even in the absence of PEI, the HA suspension exhibits a gel-like response with an elasticity (G') of $\sim 6 \times 10^4$ Pa. Upon increasing PEI additions, the ink elasticity increases, which reflects a strengthening of the gelled HA particle network. The maximum ink elasticity occurred at a [NH_x]:[COO^-] ratio of 1:2 with little further increase observed at higher PEI additions.

The minimum ink elasticity required to build a given 3-D periodic HA scaffold can be estimated using the following equation:

$$G' = 1.39 \times 10^4 \rho_{gel} g_0 \frac{L^4}{D^3}, \quad (4)$$

where ρ_{gel} is the ink density (2.05 g/cm^3), g_0 the gravitational constant, L the span length, and D the rod diameter. This expression, assumes a simply supported, elastic beam model to describe the filamentary rods, as first reported by Smay et. al. [24]. These rods can be likened to a beam with a circular cross-section that deflects (δz) under its own weight, as given by:

$$\delta z = \frac{Wy}{24EI}(2Ly^2 - y^3 - L^3), \quad (5)$$

where W is the distributed load ($= 0.25\rho_{gel} g_0 \pi D^2$), y the position along the rod, E the elastic modulus of the filament ($E = (1 + v)2G'$) [31], $v(= 0.5)$ the Poisson's ratio for the filament [32], and I the area moment of inertia of the circular cross section ($= \pi D^4/64$) [24]. A minimum needed G' of 7×10^4 Pa is predicted using this analysis for the 3-D HA scaffold ($L = 250$ μm, $D = 250$ μm) shown in Fig. 1. Concentrated HA inks ([NH_x]:[COO^-] = 0.5), which exhibit a G' of $\sim 1.2 \times 10^5$ Pa and therefore satisfy this criteria, were utilized in the direct-write assembly of the 3-D periodic HA scaffolds described below. In the absence of PEI additions, the ink-based filaments were not sufficiently

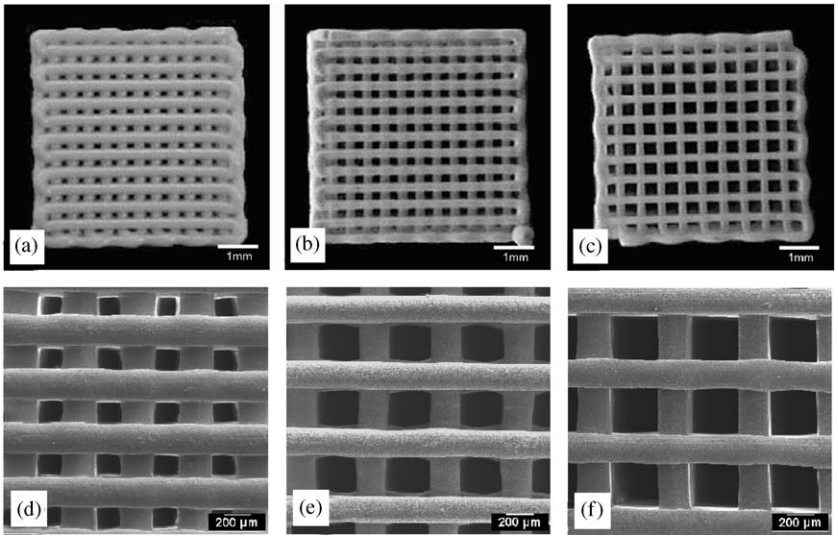

Fig. 5. Optical images of 3-D periodic hydroxyapatite scaffolds with varying minimum separation distance between rods of: (a) 250 μm, (b) 350 μm, and (c) 500 μm. And the corresponding SEM images (d–f) (top surface)

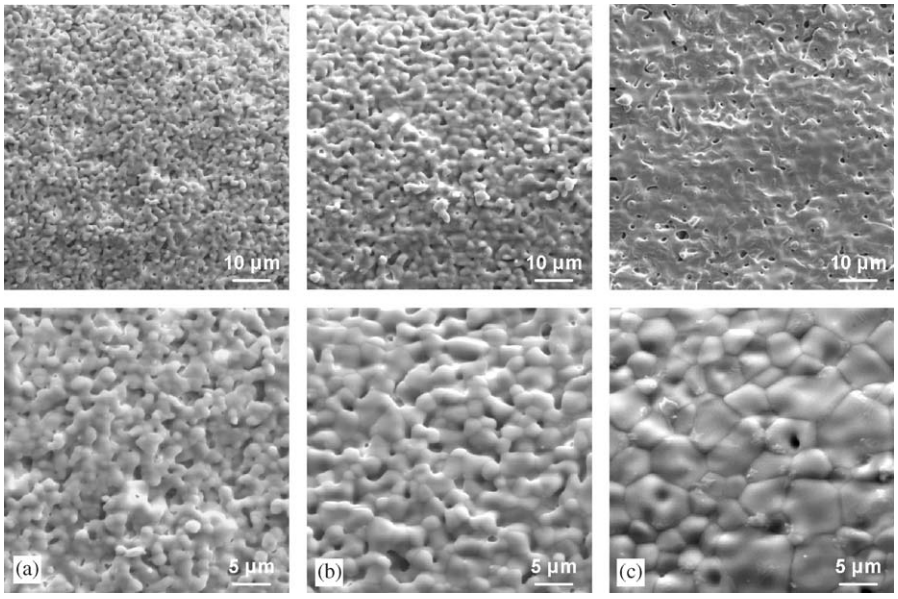

Fig. 6. SEM images of 3-D periodic hydroxyapatite scaffolds sintered at: (a) 1200 °C, (b) 1275 °C, and (c) 1300 °C, where top and bottom rows correspond to magnifications of 1000× and 2000×, respectively.

stiff to span gaps in the underlying layers without significant deformation ($\delta z > 0.05D$).

3.3. 3-D periodic HA scaffolds

3-D periodic HA scaffolds with center-to-center rod spacings of 500, 600, and 750 μm were constructed by direct-write assembly, as shown in Fig. 5. By varying the lattice (rod) spacing, HA scaffolds were produced with three-dimensionally, interconnected pore channels of varying respective sizes, D_{rod}~250, 350, and 500 μm. SEM images of the top surface of representative HA scaffolds are also shown in Fig. 5, which reveal the rod and pore channel uniformity in each of these 3-D structures.

3-D periodic HA scaffolds were sintered at varying temperatures between 1200 and 1300 °C to tailor their microporosity. Under these sintering conditions, HA ($Ca_5(PO_4)_3(OH)$) remains the dominant phase with no evidence of HA decomposition, as determined by XRD (data not shown). Fig. 6 depicts SEM micrographs of representative sintered HA scaffolds. From these microstructual images, we observed qualitatively that the number density of individual pores decreased along with a simultaneous increase in characteristic grain size with increasing sintering temperature.

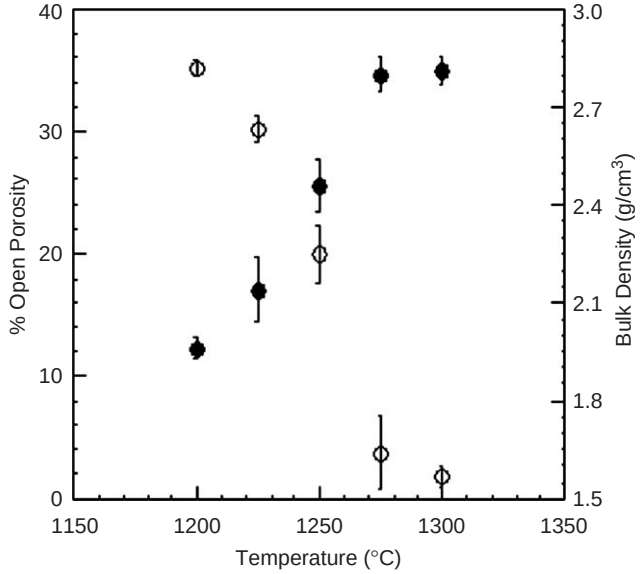

Fig. 7. Plot of open porosity (○) and bulk density (●) of hydroxyapatite structures as a function of varying sintering temperature. [Error bars denote the standard deviation in the measurements.]

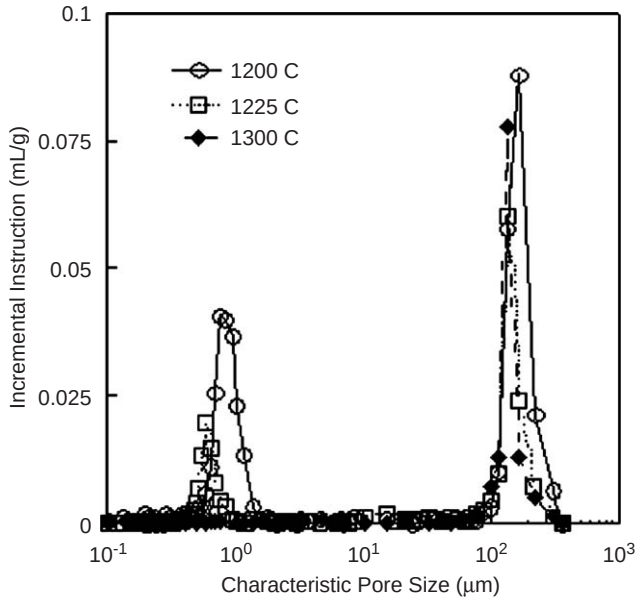

Fig. 8. Semi-log plot of pore size distribution measured for 3-D periodic hydroxyapatite scaffolds as a function of sintering temperature.

The influence of sintering temperature on the extent of open porosity (or bulk density) for solid HA structures ($D_{\text{rod}} = 0\,\mu\text{m}$) is shown in Fig. 7. As a benchmark, the as-deposited HA structure contained ~55% open porosity, in good agreement with the HA ink composition ($\phi_{\text{HA}} = 0.45$). Upon sintering to 1200 °C, there was little observed reduction in the open porosity (~40%). At 1250 °C, there was a two-fold reduction in the open porosity (~20%). The open porosity became negligible yielding a "dense" HA

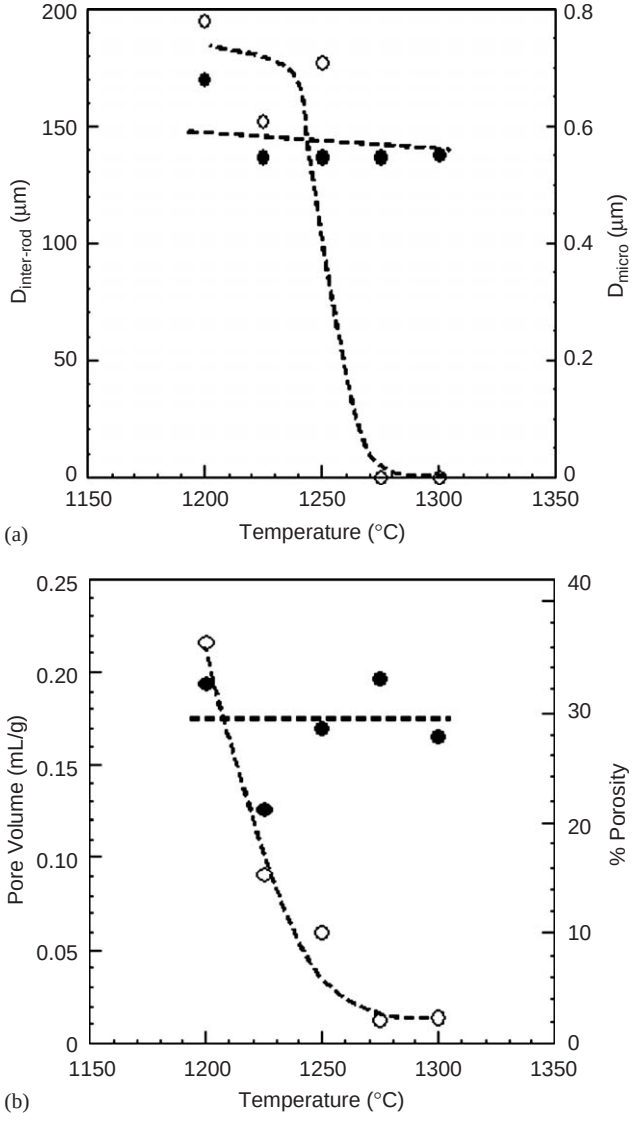

Fig. 9. Plots of: (a) characteristic pore diameter and (b) pore volume for 3-D periodic hydroxyapatite scaffolds as a function of sintering temperature, where the porosity between rods (●) and within hydroxyapatite rods (○) are shown separately.

structure (⩽2% open porosity) only after sintering at 1300 °C.

The 3-D periodic HA scaffolds sintered at varying temperatures exhibit a bimodal pore size distribution, as shown in Fig. 8. Their bimodal nature reflects contributions from both large pores stemming from the void space between HA rods within the scaffold structure and fine pores stemming from the microporosity present within individual HA rods. The characteristic size of each pore population is plotted as a function of sintering temperature in Fig. 9(a). The characteristic pore diameter between rods ($D_{\text{inter-rod}}$~150–200 μm) decreases gradually as the scaffolds shrink upon densification. In great contrast, the characteristic micropore diameter (D_{micro}) decreases abruptly at 1275 °C, which coincides with the

transition from open to closed porosity. The corresponding pore volume associated with each population of porosity within the HA scaffolds is shown in Fig. 9(b). Whether normalized by sample mass or total volume, the pore volume associated with the larger pores in the HA scaffold lattice remains nearly constant, whereas the micropore volume decreases substantially with increasing sintering temperature.

4. Conclusions

Concentrated HA inks suitable for the direct-write assembly of 3-D periodic scaffolds require both a high solids loading (~45 vol%) and high elastic shear modulus (~10^5 Pa). 3-D HA scaffolds comprised of a regular array of HA rods were fabricated. By varying the center-to-center rod spacing and sintering conditions, we developed scaffolds with a bimodal pore architecture. In a collaborative effort, in vivo studies are now underway to explore the role of HA scaffold architecture on bone ingrowth.

Acknowledgments

This material is based on work supported by the National Aeronautics and Space Administration through Grant#-NAG 8-1922. The robotic deposition apparatus used in this work was designed and built by J. Cesarano (Sandia National Laboratories, Albuquerque, NM) and the customized software for 3D fabrication was developed by J. Smay. The authors gratefully acknowledge use of the facilities in the Center for Microanalysis of Materials at the FS-MRL, which is supported by the US Department of Energy under Award No. DEFG02-91ER45439.

References

[1] LeGeros RZ. Calcium phosphate materials in restorative dentistry: a review. Adv Dent Res 1988;2(1):164–80.
[2] LeGeros RZ. Biodegradation and bioresorption of calcium phosphate ceramics. Clin Mater 1993;14:64–88.
[3] Ratner BD. Replacing and renewing: synthetic materials, biomimetics, and tissue engineering in implant dentistry. J Dent Educ 2001;65(12):1340–7.
[4] Bonfield W. Composites for bone replacement. J Biomed Eng 1988;10:522–6.
[5] Hench LL. Bioceramics: from concept to clinic. J Am Ceram Soc 1991;74(7):1487–510.
[6] Jarcho M, Kay JF, Gumaer KI, Doremus RH, Drobeck HP. Tissue, cellular, and subcellular events at a bone–ceramic hydroxylapatite interface. J Bioeng 1976;1:79–92.
[7] Gomi K, Lowenberg B, Shapiro G, Davis JE. Resorption of sintered synthetic hydroxyapatite by osteoclasts in vitro. Biomaterials 1993;14(2):91–6.
[8] Werner J, Linner-Krcmar B, Friess W, Greil P. Mechanical properties and in vitro cell compatibility of hydroxyapatite ceramics with graded pore structure. Biomaterials 2002;23:4285–94.
[9] Malinin T. Acquisition and banking of bone allografts. In: Habal MB, Hari RA, editors. Bone grafts and bone substitutes. Philadelphia: W.B. Saunders; 1992. p. 206–25.
[10] Roy DM, Linnehan SK. Hydroxyapatite formed from coral skeletal carbonate by hydrothermal exchange. Nature 1974;247:220–2.
[11] Fabbri M, Celotti GC, Ravaglioli A. Hydroxyapatite-based porous aggregates: physico-chemical nature, structure, texture, and architecture. Biomaterials 1995;16(3):225–8.
[12] Arita IH, Castano VM, Wilkinson DS. Synthesis and processing of hydroxyapatite ceramic tapes with controlled porosity. J Mater Med 1995;6:19–23.
[13] Sepulveda P. Gelcasting foams for porous ceramics. Am Ceram Soc Bull 1997;76(10):61–5.
[14] Zhao F, Yin Y, Lu WW, Leong JC, Zhang W, Zhang J, et al. Preparation and histological evaluation of biomimetic three-dimensional hydroxyapatite/chitosan-gelatin network composite scaffolds. Biomaterials 2002;23:3227–34.
[15] Ruys AJ, Wei M, Sorrell CG, Dickson MR, Brandwood A, Milthorpe BK. Sintering effects on the strength of hydroxyapatite. Biomaterials 1995;16:409–15.
[16] Rekow DE, Erdman AG, Riley D, Klamecki B. CAD/CAM for dental restorations—some of the curious challenges. IEEE Trans Biomed Eng 1991;38(4):314–8.
[17] Cima LG, Cima MJ. Preparation of medical devices by solid free-form fabrication methods. US Patent No. 5490962, 1996.
[18] Hutmacher DW. Scaffolds in tissue engineering bone and cartilage. Biomaterials 2000;21:2529–43.
[19] Langton CM, Whitehead MA, Langton DK. Development of a cancellous bone structural model by stereolithography for ultrasound characterization of the calcaneus. Med Eng Phys 1997;19:599.
[20] Chu T-MG, Orton DG, Hollister SJ, Feinberg SE, Halloran JW. Mechanical and in vivo performance of hydroxyapatite implants with controlled architectures. Biomaterials 2002;23:1283–93.
[21] Griffith LG, Naughton G. Tissue engineering—current challenges and expanding opportunities. Science 2002;295(5557):1009–14.
[22] Lewis JA, Cima MJ. Diffusivities of dialkyl phthalates in plasticized poly(vinyl butyral)—impact on binder thermolysis. J Am Ceram Soc 1990;73(9):2702–7.
[23] Cesarano J, Segalman R, Calvert P. Robocasting provides moldless fabrication from slurry deposition. Ceram Ind 1998;148:94–102.
[24] Smay JE, Cessarano III J, Lewis JA. Colloidal inks for directed assembly of 3-D periodic structures. Langmuir 2002;18(14):5429–37.
[25] Smay JE, Gratson GM, Shepherd RF, Cessarano III J, Lewis JA. Directed colloidal assembly of 3-D periodic structures. Adv Mater 2002;14(18):1279–83.
[26] Cesarano J, Aksay IA, Bleier A. Stability of aqueous alpha-Al_2O_3 suspensions with poly(methacrylic acid) polyelectrolyte. J Am Ceram Soc 1988;71(4):250–5.
[27] Wang PE, Chaki TK. Sintering behaviour and mechanical properties of hydroxyapatite and dicalcium phosphate. J Mater Sci 1993;4:150–8.
[28] Reed JS. Principles of ceramic processing. New York: Wiley; 1995.
[29] Krieger IM. Rheology of monodisperse latices. Adv Colloidal Interf Sci 1972;3:111.
[30] Rao RB, Krafcik KL, Morales AM, Lewis JA. Micro-Fabricated Deposition Nozzles for Direct Write Assembly of 3-D Periodic Structures. Adv Mater 2005;17:289–93.
[31] Shigley JE, Miskhe CR. Mechanical engineering design, 5th ed. 1989. p. 738.
[32] Channell GM, Zukoski CF. Shear and compressive rheology of aggregated alumina suspensions. AIChE J 1997;43(7):1700–8.